Total Artificial Heart Computational Fluid Dynamics: Modeling of Stator Bore Design Effects on Journal-Bearing Performance

Maryam Khelghatibana,* Mark S. Goodin,† Michael Yaksh,‡ David J. Horvath,§ Barry D. Kuban,¶ Kiyotaka Fukamachi,¶ || and Jamshid H. Karimov¶ ||

Cleveland Clinic's continuous-flow total artificial heart (CFTAH) is a double-ended centrifugal blood pump that has a single rotating assembly with an embedded magnet, which is axially and radially suspended by a balance of magnetic and hydrodynamic forces. The key to the radial suspension is a radial offset between the stator bearing bore and the magnet's steel laminations. This offset applies a radial magnetic force, which is balanced by a hydrodynamic force as the rotating assembly moves to a "force-balanced" radial position. The journal-bearing blood passage is a narrow flow path between the left and right impellers. The intent of this study was to determine the impact of the stator-bearing bore radius on the journal-bearing hydraulic performance while satisfying the geometric design constraints imposed by the pump and motor configuration. Electromagnetic forces on the journal bearing were calculated using the ANSYS EMAG program, Version 18 (ANSYS, Canonsburg, PA). ANSYS CFX Version 19.2 was then used to model the journal-bearing flow paths of the most recent design of the CFTAH. A transient, moving mesh approach was used to locate the steady state, force-balanced position of the rotating assembly. The blood was modeled as a non-Newtonian fluid. The computational fluid dynamics simulations showed that by increasing stator bore radius, rotor power, stator wall average shear stress, and blood residence time in journal-bearing decrease, while blood net flow rate through the bearing increases. The results were used to select a new bearing design that provides an improved performance compared with the baseline design. The performance of the new CFTAH-bearing design will be confirmed through upcoming *in vitro* and *in vivo* testing. *ASAIO Journal* 2022; 68;655–662

Key Words: computational fluid dynamics, total artificial heart, continuous flow, hydrodynamic bearing, simulation

From the *SimuTech Group, Montreal, Quebec, Canada; †SimuTech Group, Hudson, Ohio; ‡Yaksh Magnetic Solutions, Lilburn, Georgia; §R1 Engineering, LLC, Euclid, Ohio; ¶Department of Biomedical Engineering, Lerner Research Institute, Cleveland Clinic, Cleveland, Ohio; and ||Cleveland Clinic Lerner College of Medicine of Case Western Reserve University, Cleveland Clinic, Cleveland, Ohio.

Submitted for consideration December 2020; accepted for publication in revised form June 2021.

Disclosure: D.J. Horvath and B.D. Kuban are coinventors of the device. The other authors have no conflicts of interest to report.

This work was supported with federal funding obtained from the National Heart, Lung and Blood Institute, National Institutes of Health (Bethesda, Maryland), under grant 5R01HL096619.

Correspondence: Jamshid H. Karimov, Department of Biomedical Engineering/ND20, Cleveland Clinic, 9500 Euclid Avenue, Cleveland, OH 44195. Email: karimoj@ccf.org

DOI: 10.1097/MAT.0000000000001556

Heart failure (HF) is a serious healthcare issue, affecting more than 20 million people worldwide,[1,2] and is a primary contributor to cardiovascular mortality. In the United States alone, by 2030, > 8 million people (1 in every 33) are projected to have HF. The prevalence of advanced-stage heart disease is rising rapidly, affecting more of elderly Americans hospitalized for HF than for any other medical condition.[3] Heart transplantation can provide a remarkable improvement in quality of life and survival in selected patients with end-stage HF,[4,5] but a shortage of donor hearts will always limit this option.

Technologies intended for durable mechanical circulatory support (MCS) are considered as replacement therapy for advanced-stage cardiac disease because of the lack of organ donation. The recent success of continuous-flow (CF) circulatory support devices has led to the growing acceptance of these devices as a viable therapeutic option for end-stage HF patients who are not responsive to any existing drug or electrophysiologic treatment.[6] The modern, CF MCS-based therapy is realized as an implantation of a blood pump with a rotor bearing necessary to ensure its reliability during extended operation.[7] Due to their simple structure and low power consumption, blood pumps with hydrodynamic bearings are making their way into clinical applications. Such hydrodynamically suspended rotary blood pumps with noncontact bearings are particularly effective at enhancing blood compatibility.[7,8]

Cleveland Clinic's CF total artificial heart (CFTAH) is a double-ended centrifugal blood pump and is composed of a single rotating assembly. The right impeller sends the blood coming from the body through the right atrium to the lungs. The left impeller receives the oxygenated blood from the lungs through the left atrium and pumps it throughout the body. The journal-bearing blood passage is a thin, cylindrical region with a nominal radial clearance of 0.004 inches that connects the left and right impeller regions (Figure 1). Its role is to support the rotating assembly and to provide the hydraulic radial force for the hydrodynamic bearing.[9]

The left impeller is composed of six primary and six smaller splitter blades and provides a hydraulic pressure head of 60 to 110 mm Hg over its operating range which is 3 to 8 L/min. The right impeller has seven primary blades without splitters, and it supplies a hydraulic pressure head of 20 to 40 mm Hg.

The rotating assembly has an embedded magnet that is shorter than the motor's steel laminations.[10] This difference in length allows a degree of free axial movement in the direction of net axial force that is primarily caused by an imbalance of pump inlet (atrial) pressures. The range of relatively free axial movement is bounded by increasing magnetic axial stiffness, which acts to restrain excess movement of the rotor. An aperture that opens and closes with axial movement of the rotor connects the right pump impeller section with the right volute. The aperture allows the rotating assembly to move axially to a

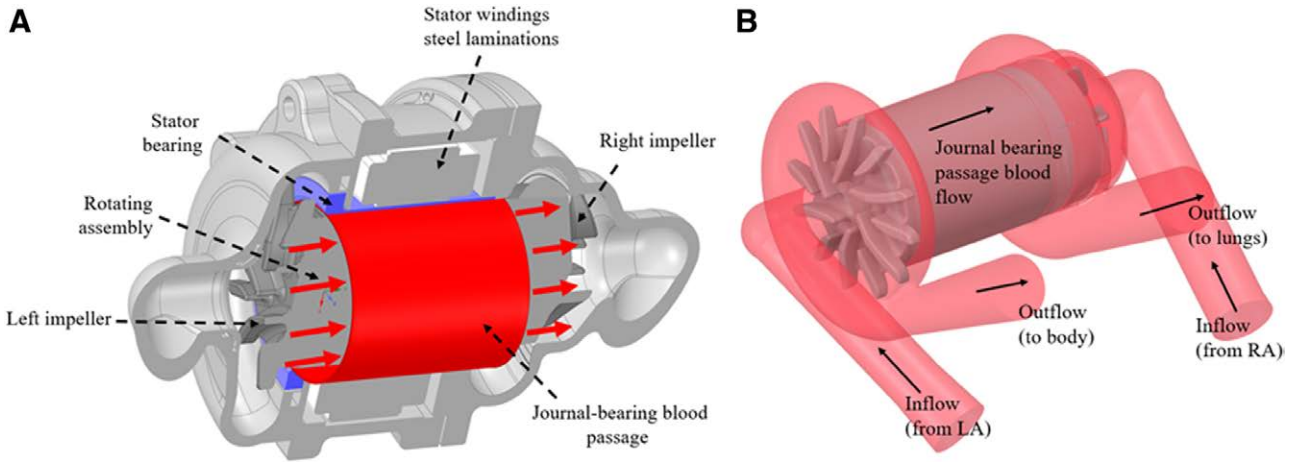

Figure 1. CFTAH100 design. (**A**) Cross section showing main components; (**B**) blood passage including the thin connecting journal-bearing flow path. CFTAH, continuous-flow total artificial heart.

magnetic/hydraulic "force-balanced" axial position.[11] This self-pressure regulation of the pump through automatic adjustment of the aperture has been reported previously.[12]

The focus of the current work is the radial suspension of the rotating assembly. The rotating assembly derives lift from its own motion, creating a hydrodynamic bearing force that requires stabilization. The key to the radial stabilization is a radial offset between the stator-bearing bore and the motor winding's steel laminations. This offset applies a radial magnetic force that counteracts the hydrodynamic force as the rotating assembly moves to a "force-balanced" radial position (Figure 2).

Cleveland Clinic has built and tested an earlier design, the CFTAH080, whose journal-bearing design was found acceptable in terms of hydrodynamic stability and biocompatibility.[12] However, the CFTAH080 had a lower-than-desired axial stiffness and, correspondingly, higher-than-desired axial travel. Therefore, a new design, the CFTAH100, which has a similar bearing configuration as the CFTAH080, was proposed. The CFTAH100 incorporates a new stacked magnet that offers an increased axial magnetic stiffness. However, the radial magnetic stiffness of the CFTAH100 is reduced due to the gap between the split magnets and an overall shorter total magnet length.[13] A lower radial magnetic stiffness increases the risk of

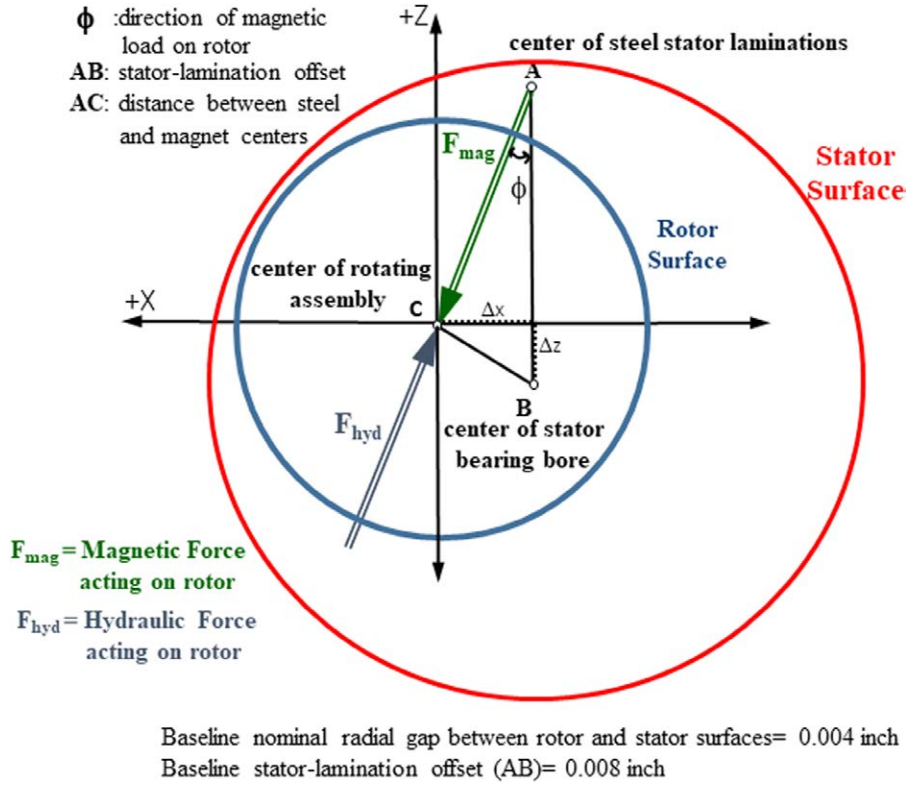

Figure 2. Illustration of continuous-flow total artificial heart (CFTAH) journal-bearing force-balanced angular relationships.

rotor instability (the rotor bouncing around within the bearing clearance), causing reliability issues and potentially reduced biocompatibility.

To improve the stability of the CFTAH100, two parameters were identified: lamination-stator offset and bearing radial clearance. A larger lamination-stator offset results in a higher magnetic force, hence improved stability. Moreover, higher radial clearance makes the rotor assembly more stable by lowering the potential of the hydrodynamic lift surpassing the magnetic load. Therefore, the goals of this study were to first determine a lamination-stator offset to radially stabilize the rotating assembly, and then to evaluate the impact of different radial clearances on the bearing's overall performance. As the CFTAH080 journal-bearing performance was radially stable and provided the desired hydraulic performance and biocompatibility, it was used as a reference point for the current study.

Methods

Electromagnetics Model

The ANSYS EMAG Version 18 program (ANSYS, Canonsburg, PA) was used to simulate the magnetic field in the CFTAH100 pump. The three-dimensional finite element model of the dual rotor and stator motor allowed the rotor to rotate and to move radially independent of the stator, which allowed us to determine the magnetic rotor stiffness. A mesh study was conducted on a prior CFTAH design which had a longer magnet length compared with CFTAH100.[11] This study showed that increasing the number of elements from 148,188 elements to 541,902 resulted in less than 5% variation in force and torque. Based on this study, a finite element model composed of 308,000 hexahedral elements was generated for CFTAH100. Due to the strength of the rare earth magnets, the material model for the permeable components (iron) accounted for the field saturation in the iron. The rare earth magnets need only a linear material model. The direction of the modeled magnetization corresponded to the parallel magnetization of the physical permanent magnet.

As the rotor was displaced, the magnet field was also shifted. Sufficient air (free space) outside the pump was also modeled to account for the effect of the magnetic field leakage at all the faces of the pump that could most affect the radial stiffness calculation. The finite element mesh in the air gap was composed of hexahedral elements positioned in such a manner that the rotor displacement (increasing the radial gap on one side of the rotor while decreasing the gap on the opposite side) would not result in distorted elements.

Figure 3A shows the magnetic flux density of the motor for the centered position of the rotor. A detailed view of the field for the rotor at the maximum 0.014 inches radial displacement is also shown in Figure 3B (the range of flux density was adjusted in order to clearly illustrate the differences of flux density between the right and the left side of the figure). The radial displacement allows the field on the side of the rotor with the decreased gap to be increased, with an associated increase of force, while the opposite side experiences a decreased field with a lower force. Such a differential results in a net force pulling the rotor in the direction to further decrease the gap. The radial displacement does not significantly change the direction of the net force but does result in an increase in net force. Since the magnetic properties remain basically linear, the net force is also essentially linear. Using a radial displacement of 0.014 inches, the resulting magnetic radial stiffness is determined to be 680 N/inch (Figure 4).

Computational Fluid Dynamics Model

The ANSYS CFX Version 19.2 program (ANSYS, Canonsburg, PA) was used to model the journal-bearing flow paths. In the previous computational fluid dynamics (CFD) studies of the entire CFTAH100 pump blood flow path, the forces acting within the journal-bearing region accounted for more than

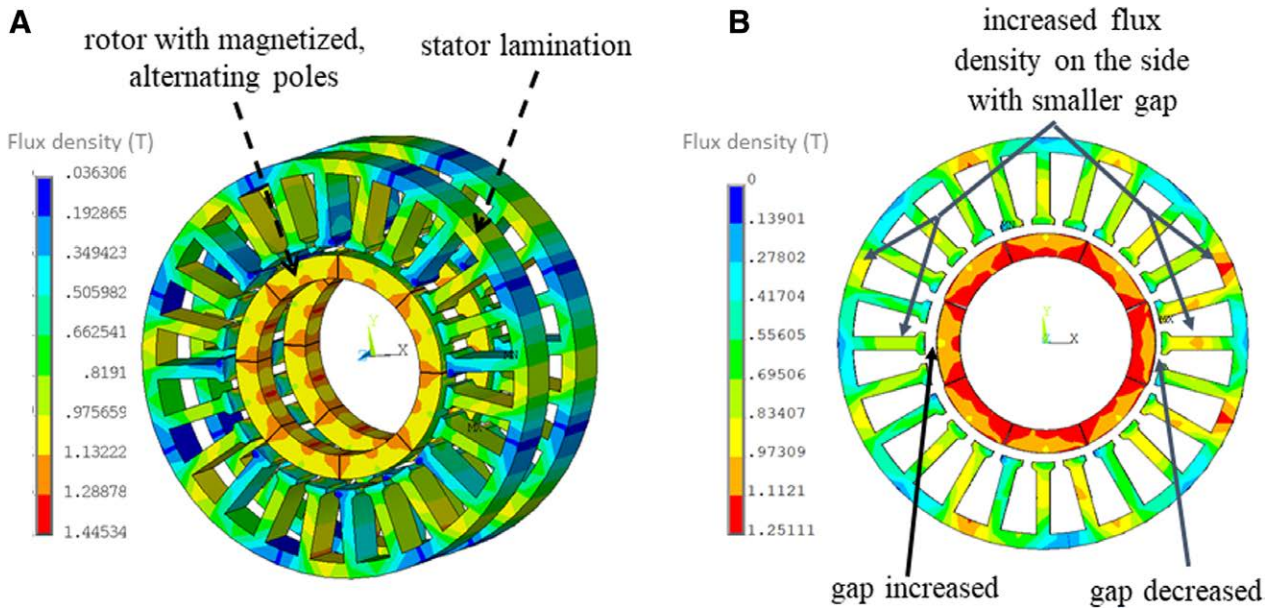

Figure 3. Magnetic field of the motor. (**A**) Rotor at the centered position with respect to the stator; (**B**) rotor moved radially from the centered position by 0.014 inches.

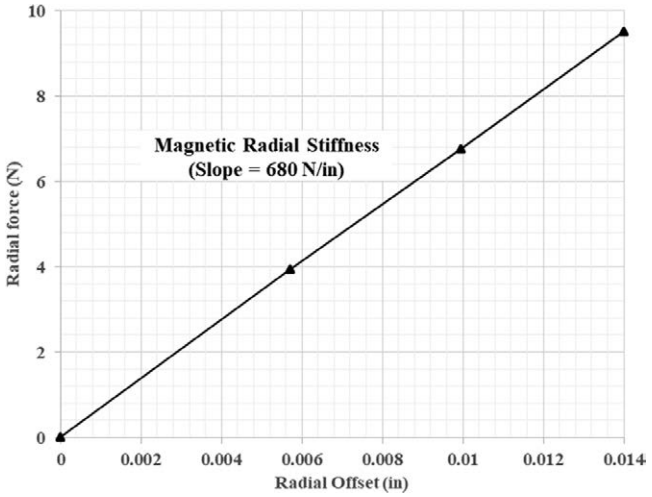

Figure 4. Motor radial magnetic force *vs.* radial offset.

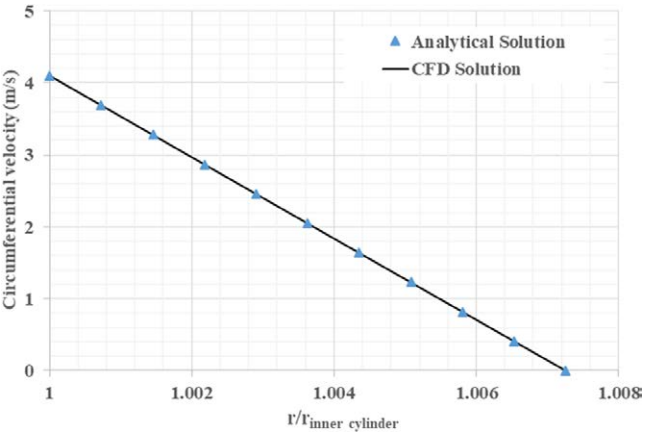

Figure 5. Circumferential velocity between two concentric cylinders with inner cylinder rotating around the axis of the cylinder-analytical solution *vs*. computational fluid dynamics (CFD).

90% of the radial hydraulic forces. Leveraging this knowledge, the journal-bearing fluid volume was extracted from the three-dimensional geometry of CFTAH100 and modeled for these studies. The ANSYS-Meshing program was used to create a hexahedral mesh. A mesh study was required to ensure that CFD results are independent of mesh refinement. Therefore, the mesh was refined in the computational grids from mesh M1 to mesh M4 by doubling the number of elements in each direction (axial, radial, and circumferential) for every refinement step.

Table 1 presents the variation of hydraulic forces, average stator wall shear stress and rotor displacement relative to bearing bore axis at forced-balanced position with mesh refinement. Based on this study, mesh M3 with 528,000 elements, including 11 elements across the journal-bearing fluid gap, was selected, as it provided the same force-balanced position of the rotor as the most-refined mesh M4. The blood was modeled as a non-Newtonian fluid,[14–16] with a viscosity of 3.5 cP at a shear strain rate of 40,000 s^{-1}. The density of the blood was assumed to be 1,060 kg/m^3. A nominal pressure difference of 20 mm Hg, based upon previous CFTAH100 full pump CFD modeling results, was applied across the bearing.[11]

Table 1. Continuous-Flow Total Artificial Heart Journal-Bearing Computational Fluid Dynamics Mesh Study

	Mesh M1	Mesh M2	Mesh M3	Mesh M4
Number of elements	9,000	72,000	528,000	4,224,000
Hydraulic force-X component (N)	0.80	0.81	0.80	0.80
Hydraulic force-Z component (N)	8.80	8.81	8.80	8.80
Stator wall average wall shear stress (dyne/cm^2)	1,327	1,334	1,327	1,325
Rotor displacement relative to bearing bore axis at forced-balanced position in X direction (in)	0.00130	0.00119	0.00118	0.00118
Rotor displacement relative to bearing bore axis at forced-balanced position in Z direction (in)	0.000401	0.000352	0.000360	0.000360

The CFD model of journal bearing was verified by comparing CFD results with an analytical solution of flow between two long concentric rotating cylinders.[17] The CFD model used for analytical comparison was composed of two concentric cylindrical walls with the inner wall rotating around the axis of the cylinder. Symmetry boundary conditions were assigned to both ends of the cylinders to prevent introducing end-wall effects. The working fluid was set to blood with a constant viscosity of 3.5 cP and a density of 1,060 kg/m^3. Mesh resolution, CFD solver parameters and convergence criteria of the verification model were identical to those of CFTAH100 CFD model. The CFD results for circumferential velocity in the gap (Figure 5) as well as wall shear stresses and torques matched very well with analytical solution (Table 2).

The journal-bearing model created in ANSYS consisted of the rotor wall spinning around a fixed axis and radially moving stator walls. This motion is opposite the actual bearing motion, with fixed stator walls and spinning rotor walls moving inward/outward. However, this approach simplified the CFD modeling, allowing for the computational domain to spin around a fixed axis. A transient, moving mesh approach was used to locate the steady state, force-balanced position of the rotating assembly. A set of user-defined expressions using CFX expression language was used to update the radial position of stator walls until a "force-balanced" position was reached.

To improve the performance of the CFTAH100 journal bearing, the radial lamination-stator offset was modified so that the main characteristics of the successful CFTAH080 bearing, in terms of pressure loads, wall shear stress, and flow residence time, were replicated with the new CFTAH100 design. For comparison with the previous CFTAH080-bearing simulation

Table 2. Flow Between Two Concentric Rotating Cylinders-Comparison Between Analytical Solution and Computational Fluid Dynamics

	Inner Cylinder Wall Shear Stress (dyne/cm^2)	Outer Cylinder Wall Shear Stress (dyne/cm^2)	Torque (oz.in)
Analytical solution	1,408	1,429	7.5
CFD solution	1,408	1,429	7.5
Difference	0%	0%	0%

results, the pump's nominal rotational speed of 2,800 rpm and peak rotational speed of 3,600 rpm were again selected for the current models. Using the new lamination-stator offset, the influence of bearing clearance on rotor power and the main characteristics of the bearing blood flow were investigated.

Experimental measurements cannot be performed in the thin blood flow path of journal bearing because of its configuration and location. Therefore, to ensure equivalency of the bearing parameters, the same CFD method was used to design the bearings for the CFTAH080 and CFTAH100 pumps and their prior designs. The coupled EMAG/CFD full pump model of a precedent design of CFTAH080 was verified against experimental data.[11]

Results

In this study, the lamination-stator offset of the CFTAH100 was increased from the original value of 0.008 inches in the CFTAH080 to 0.0133 inches. Further increases in the lamination-stator offset are bounded by fabrication constraints. Figure 6A shows the static pressures on the stator walls for the CFTAH080 and CFTAH100 designs with the two aforementioned offset values. The CFTAH100 with the original CFTAH080 offset of 0.008 inches was too lightly loaded and therefore susceptible to radial instability. Increasing the lamination-stator offset to 0.0133 inches resulted in an increased radial loading on the stator, closely matching the original CFTAH080 results, and providing improved hydrodynamic stability.

Patterns in wall shear stress can indicate regions that are susceptible to hemolysis or thrombus formation. The stator wall shear stresses are compared for the three cases modeled with differing lamination-stator offsets (Figure 6B). This figure shows that wall shear stress distribution of the CFTAH100 with the new, larger offset of 0.0133 inches closely matches that of the CFTAH080 with its smaller 0.008 inches offset.

Likewise, Figure 6C compares the flow residence time for the three simulated cases. By increasing the lamination-stator offset to 0.0133 inches, residence time for the CFTAH100 was reduced by 30% and closely matched that of the CFTAH080 design.

With the new lamination-stator offset of 0.0133 inches, the radial clearance of the CFTAH100 was varied from 0.003 inches to 0.007 inches for the pump running at a rotational speed of 2,800 rpm. The nominal clearance for the CFTAH080 design was 0.004 inches.

Bearing power loss is shown in Figure 7A. At a constant pump rotational speed, the bearing power loss decreases with the increase in the nominal radial clearance. This results in the generation of less heat within the fluid film of blood.

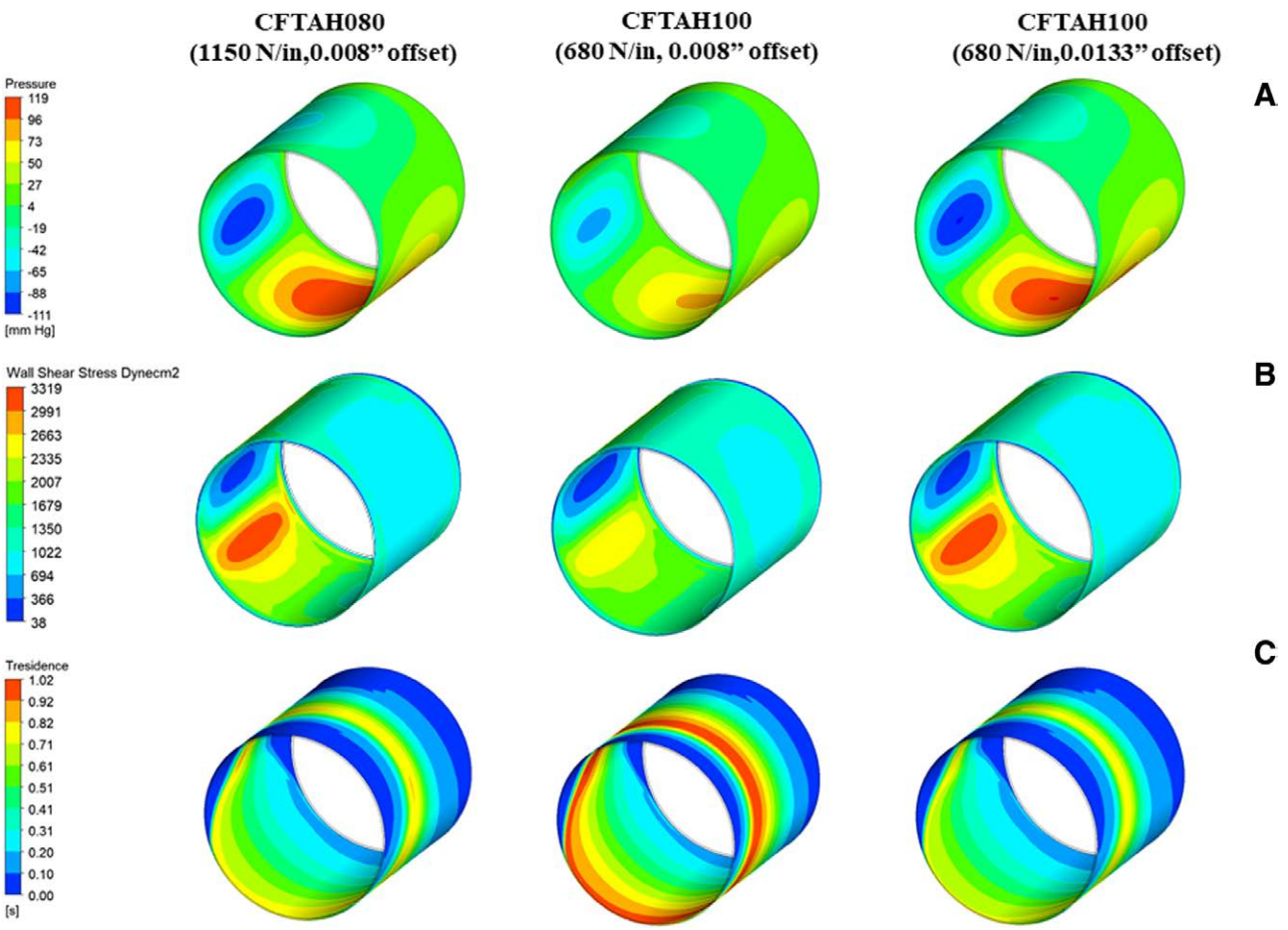

Figure 6. CFTAH080 *vs*. CFTAH100. (**A**) static pressures on the stator walls; (**B**) wall shear stress on the stator walls; and (**C**) blood flow residence time on a surface offset from the stator wall. CFTAH, continuous-flow total artificial heart.

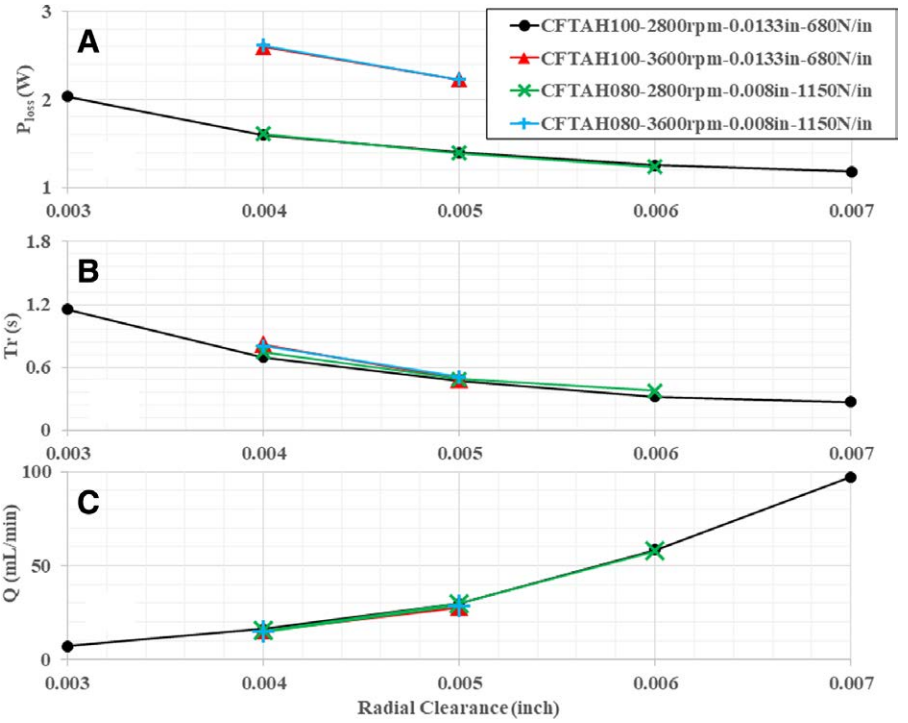

Figure 7. Effect of nominal radial clearance and pump rotational speed, Part 1 of 2: (**A**) journal-bearing power loss (P_{loss}); (**B**) blood maximum residence time in journal bearing (Tr); and (**C**) net blood flow rate through journal bearing (Q).

Figure 7B shows that at a constant pump rotational speed with increasing nominal radial clearance, maximum residence time decreases. This is advantageous, because the blood is exposed to the elevated bearing shear stress levels for a shorter duration, thus reducing the likelihood of hemolysis.[18]

Figure 7C illustrates that at a constant pump rotational speed, bearing axial shunt flow increases as nominal radial clearance increases. Flow rate in the bearing is small, but increased flow rate is good for improved bearing washout and reducing the potential for thrombus formation.

Stator wall average and maximum shear stresses are illustrated in Figure 8. The average wall shear stress decreases with increasing nominal radial clearance. However, the maximum wall shear is minimized with a nominal radial clearance of 0.004 inches at 2,800 rpm. A higher wall shear stress could increase the potential of hemolysis.

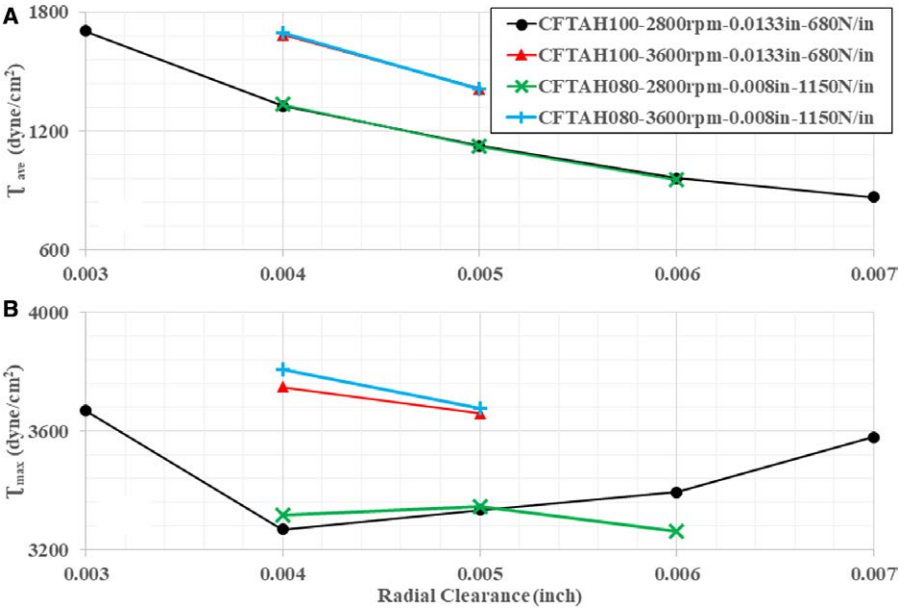

Figure 8. Effect of nominal radial clearance and pump rotational speed, Part 2 of 2: (**A**) stator wall average shear stress (τ_{ave}) and (**B**) stator wall maximum shear stress (τ_{max}).

Figures 7 and 8 also compare performance of the CFTAH100 with 0.0133 inches lamination-stator offset at 0.004, 0.005, and 0.006 inches clearance with that of CFTAH080. This comparison confirms that the CFTAH100 with the new lamination-stator offset presents a similar performance, in terms of bearing power loss, blood residence time, bearing axial shunt flow, and stator wall shear stress, as the CFTAH080.

As mentioned earlier, we intend to further improve the radial stability of the CFTAH100 journal bearing by increasing radial clearance. However, excessively opening up the radial clearance can itself cause instability, as the rotor will have more room to bounce around. Therefore, although based on the radial clearance study at 2,800 rpm, a higher radial clearance presents lower power loss, blood residence time and average wall shear stress, a radial clearance of 0.005 inches was selected for further analysis. This radial clearance provides an overall improved performance compared with that of 0.004 inches while maintaining a desirable opening for journal-bearing radial clearance.

The performance of the CFTAH100 journal bearing with the new lamination-stator offset was also investigated at the maximum intended rotational speed of 3,600 rpm for both 0.004 and 0.005 inches radial clearances. The CFTAH100 results were compared with CFTAH080's performance at 0.004 and 0.005 inches radial clearance and 3,600 rpm to ensure that at an elevated rotational speed, the performance of the two bearings was comparable (Figures 7 and 8).

Figure 7A shows that increasing rotational speed of CFTAH100 from 2,800 rpm to 3,600 rpm results in a 60% increase in bearing power loss. Blood maximum residence time in the journal bearing increases by 18% at 0.004 inches and remains almost the same at 0.005 inches (Figure 7B). Increasing rotational speed does not significantly impact the blood net flow rate through journal bearing (Figure 7C). Both stator wall average and maximum shear stresses increase by increasing rotational speed (Figure 8). However, all of the aforementioned performance parameters of journal bearing for CFTAH100 with the new lamination-stator offset were similar to those of CFTAH080 at 3,600 rpm.

Discussion

Hydrodynamic bearings are low-clearance, purely passive-type bearings, and their bearing gap is designed to be dependent on the bearing load. The bearing film requires a dynamic pressure buildup that is usually generated by means of a decreasing gap. Different types of bearings provide this pressure buildup in different ways. For example, in journal bearings, this is generally caused by an eccentric shaft, while in Mitchell-type thrust bearings, multiple wedges fulfill this task. Disadvantages are the very small gaps, which lead to high fluid friction and high shear stresses that may initiate hemolysis. Also, due to reduced gaps, high precision machining is required.[19]

Minor manufacturing inconsistencies can play a large role in unstable journal-bearing operations.[20] Unlike their rolling element counterparts (*i.e.*, ball bearings), there is an optimal size for a journal bearing under a given application. If the bearing is too small for its application, the journal may experience bearing rub due to inadequate radial clearance between the journal and the bearing. If the bearing is too large for its application, unstable orbital motion can cause the journal to move progressively off-center until it contacts the bearing. Regardless of the cause, bearing rub increases friction and heat generation between the moving parts, eventually presenting as a transient or permanent increase in the electric current drawn by the motor.

Through speed modulation, the CFTAH is intended to provide pulsatile characteristics in the actual clinical application, which may affect the suspension performance of the journal bearing under various hemodynamic conditions. In our work, the effects of pulsatile flow pattern on suspension force from the CFTAH was not specifically explored due to the unlimited number of potential pulsatile flow conditions. However, the performance of the two bearing designs was evaluated and was very comparable at nominal and maximum rotational speed conditions.

The CFTAH080, an earlier design of the Cleveland Clinic CFTAH, showed more than desired axial movement of the rotating assembly during extreme operating conditions, typically encountered during implantation surgery. Therefore, a new design, CFTAH100, was proposed, with a stacked magnet to provide increased axial stiffness. However, this stacked motor design, with its shorter overall total magnet length, has a lower radial stiffness compared with the CFTAH080. The main goals of this study were to 1) find a lamination-stator offset that increases the bearing loading and improves the radial stability of the CFTAH100 design; and 2) select a nominal radial clearance for the CFTAH100 design that reduces the potential of blood damage in the journal bearing by mimicking the performance of the successful CFTAH080 design.

The existing work on performance of the journal bearing is primarily focused on the suspension performance under CF conditions, where hydrodynamic bearing models were tested with given constant flow rate, speed, and bearing differential pressure representing the expected nominal for clinical operation. However, in the actual clinical application, the inlet and outlet pressures of the CFTAH would vary according to the periodic pressure change of the entire atrial balance and pressure distributions within the device-vasculature system and would also be affected by compliances of the connected aorta and pulmonary tree. Thus, the characteristics on the suspension performance of the proposed journal bearing will be dynamically adjusted. Because the scales of lubrication films and groove depths are on the order of micrometers, the blood in the gap should be updated continuously, and the corresponding flow rate should be as large as possible in order to improve washout.[21,22] The selection of radial clearance for the CFTAH has been made to minimize peak shear stress and not to maximize bearing net flow.

A coupled EMAG/CFD approach was used to find the force balance position for each design iteration. A sensitivity study was performed in an EMAG simulation to predict how radial magnetic force varies with rotor displacement. This relation was then used in an iterative CFD simulation that calculated the hydraulic forces and determined the force-balanced position of the rotor. A set of CFD simulations were carried out to compare a range of journal-bearing designs with respect to different performance parameters, such as power loss, blood residence time, flow rate, and shear stress. A final design that offers the most suitable compromise between different performance parameters and fabrication constraints was selected. However, the effects of hemolysis and thrombotic formations within the pump gaps or blood-contacting surfaces are still to be verified using the advanced CFD techniques and validated *in vivo*.

Conclusions

Based on the results of this study, a lamination-stator offset of 0.0133 inches was selected for the CFTAH100. This offset offers a larger bearing load, increased radial stability and similar performance with regard to shear stress and residence time to that of the CFTAH080 that was tested and found acceptable in terms of stability and biocompatibility. With the new lamination-stator offset, a radial clearance of 0.005 inches was selected for the CFTAH100. This radial clearance offers lower power loss, lower average residence time, increased bearing flow rate, lower average stator wall shear stress, and comparable peak stator wall shear stress compared with the CFTAH080 design. It is also anticipated that the CFTAH100 bearing design will offer the desired radial stability as that provided by the CFTAH080 design. *In vitro* hemolysis testing and *in vivo* animal evaluations of the CFTAH100 with the new bearing design are ongoing to demonstrate its overall performance, including stability and hemocompatibility.

Acknowledgment

D.J. Horvath conceived the research idea and provided guidance concerning design parameter selections and results interpretation. J.H. Karimov and K. Fukamachi supervised and coordinated the research. M. Khelghatibana and M.S. Goodin developed the methods and conducted the CFD analyses. M. Yaksh conducted the EMAG analyses. J.H. Karimov, K. Fukamachi, D.J. Horvath and M.S. Goodin are responsible for the literature search. M. Khelghatibana and M. Yaksh wrote the manuscript with input from all authors. All authors performed a critical review of the article and provided feedback.

References

1. Benjamin EJ, Virani SS, Callaway CW, *et al*; American Heart Association Council on Epidemiology and Prevention Statistics Committee and Stroke Statistics Subcommittee: Heart disease and stroke statistics-2018 update: A report from the American Heart Association. *Circulation* 137: e67–e492, 2018.
2. Benjamin EJ, Muntner P, Alonso A, *et al*; American Heart Association Council on Epidemiology and Prevention Statistics Committee and Stroke Statistics Subcommittee: Heart disease and stroke statistics-2019 update: A report from the American Heart Association. *Circulation* 139: e56–e528, 2019.
3. Heidenreich PA, Albert NM, Allen LA, *et al*; American Heart Association Advocacy Coordinating Committee; Council on Arteriosclerosis, Thrombosis and Vascular Biology; Council on Cardiovascular Radiology and Intervention; Council on Clinical Cardiology; Council on Epidemiology and Prevention; Stroke Council: Forecasting the impact of heart failure in the United States: A policy statement from the American Heart Association. *Circ Heart Fail* 6: 606–619, 2013.
4. Wever-Pinzon O, Drakos SG, Kfoury AG, *et al*: Morbidity and mortality in heart transplant candidates supported with mechanical circulatory support: Is reappraisal of the current United network for organ sharing thoracic organ allocation policy justified? *Circulation* 127: 452–462, 2013.
5. Garbade J, Bittner HB, Barten MJ, Mohr FW: Current trends in implantable left ventricular assist devices. *Cardiol Res Pract* 2011: 290561, 2011.
6. Moazami N, Fukamachi K, Kobayashi M, *et al*: Axial and centrifugal continuous-flow rotary pumps: A translation from pump mechanics to clinical practice. *J Heart Lung Transplant* 32: 1–11, 2013.
7. Fu Y, Hu Y, Huang F, Zhou M: The impact of pulsatile flow on suspension force for hydrodynamically levitated blood pump. *J Healthc Eng* 2019: 8065920, 2019.
8. Moazami N, Hoercher KJ, Fukamachi K, *et al*: Mechanical circulatory support for heart failure: Past, present and a look at the future. *Expert Rev Med Devices* 10: 55–71, 2013.
9. Fukamachi K KJ, Horvath D, Byram N, Goodin M: Impeller for artificial heart blood pumps. WIPO.
10. Fukamachi K, Horvath DJ, Massiello AL, *et al*: An innovative, sensorless, pulsatile, continuous-flow total artificial heart: Device design and initial *in vitro* study. *J Heart Lung Transplant* 29: 13–20, 2010.
11. Kobayashi M, Horvath DJ, Mielke N, *et al*: Progress on the design and development of the continuous-flow total artificial heart. *Artif Organs* 36: 705–713, 2012.
12. Karimov JH, Moazami N, Kobayashi M, *et al*: First report of 90-day support of 2 calves with a continuous-flow total artificial heart. *J Thorac Cardiovasc Surg* 150: 687–693.e1, 2015.
13. Kuban BD, Karimov JH, Miyamoto T, *et al*: Total artificial heart incorporating novel stacked motor; first *in vivo* results. J Heart Lung Transplant 39: S413, 2020.
14. Cross MM. Rheology of non-Newtonian fluids—a new flow equation for pseudoplastic systems. J Colloid Sci 20: 417–437, 1965.
15. Cho YI, Kensey KR: Effects of the non-Newtonian viscosity of blood on flows in a diseased arterial vessel. Part 1: Steady flows. *Biorheology* 28: 241–262, 1991.
16. Banerjee RK, Cho YI, Kensey K: Effect of non-Newtonian viscosity of blood on steady and pulsatile flow in stenosed arteries. Adv Bioeng 20: 103–106, 1991.
17. White FM. Fluid Mechanics. 7th ed. New York: McGraw-Hill, 2011.
18. Leverett LB, Hellums JD, Alfrey CP, Lynch EC: Red blood cell damage by shear stress. *Biophys J* 12: 257–273, 1972.
19. Kink T, Reul H: Concept for a new hydrodynamic blood bearing for miniature blood pumps. *Artif Organs* 28: 916–920, 2004.
20. Ranganath NK, Rashidi M, Antaki JF, *et al*: Mechanical blood-immersed bearings in continuous-flow rotary blood pumps. *ASAIO J* 66: 343–347, 2020.
21. Han Q, Zou J, Ruan X, Fu X, Yang H: A novel design of spiral groove bearing in a hydrodynamically levitated centrifugal rotary blood pump. *Artif Organs* 36: 739–746, 2012.
22. Murashige T, Sakota D, Kosaka R, *et al*: Plasma skimming in a spiral groove bearing of a centrifugal blood pump. *Artif Organs* 40: 856–866, 2016.